文章编号：1001－9014(2017)06－0655－05 DOI:10.11972/j.issn.1001－9014.2017.06.004

Grating rectangular waveguide for THz backward wave oscillator

ZHANG Kai-Chun*, CHEN Ke, WANG Qi, SHENG Chang-Jian, YUAN Xue-Song

(THz Center, School of Physical Electronics, University of Electronic Science and Technology of China, Chengdu 610054, China)

Abstract: A slow-wave structure (SWS) composed of a grating inside a rectangular waveguide is adopted as the circuit of the backward wave oscillator (BWO) in terahertz regime in this paper. Its dispersion curves and interaction impedance are presented by an analytical method and three-dimensional (3-D) electromagnetic software. The results by analysis and simulation agree well. By optimization, a BWO with the SWS at a central frequency 340 GHz is fully verified by 3-D particle-in-cell (PIC) code. The BWO is demonstrated with more than 100 mW output power at very low current density and 30 GHz tuning bandwidth.

Key words: backward wave oscillator (BWO), rectangular waveguide grating, slow-wave structure (SWS), terahertz

PACS: 94.05.Pt, 41.20.Jb, 84.40.Fe

矩形波导加载光栅结构的太赫兹振荡器

张开春*, 陈 科, 王 奇, 盛昌建, 袁学松

(电子科技大学 物理电子学院太赫兹中心,四川 成都 610054)

摘要:采用矩形波导加载光栅的慢波结构作为太赫兹返波管的高频结构,通过理论分析和电磁仿真研究了该慢波结构的色散特性和互作用阻抗,理论分析结果和仿真结果能很好地吻合.在理论分析的基础上,设计了一个中心频率为340 GHz的返波管,经粒子模拟软件计算,在较低电流密度的情况下该返波管输出功率达100 mW且可调带宽约30 GHz.

关 键 词:返波管;矩形波导光栅;慢波结构;太赫兹

中图分类号:O45,O46,TN1 **文献标识码**:A

Introduction

The application of THz wave, which has been sprung out recently in the field of communication, security, imaging, medicine and many others, promotes the development in THz sources. The vacuum terahertz sources[1-6] are recognized as the promising sources, especially compact and powerful THz sources. This type of sources is a challenging issue due to the high level of losses and the small dimensions that makes it very difficult to design and realize the source. Recently, advances in micro-fabrication techniques and electron guns have greatly promoted the development of terahertz vacuum electron devices. A 650 GHz micro-fabricated BWO based on a folded waveguide was reported with 52mW output power[7], but the current density 1 000 A/cm^2 was so high that it was very difficult to control. A BWO at 1THz supported by European Community FP7 OPTHER Project was performed[8]. An output power of 75 mW was predicted with the current density about 200 A/cm^2. These sources require very high current density so that it is difficult to design and realize.

The frequency near 340 GHz is an important atmosphere window so that it can be applied for wireless communication system[9-11]. Some applications of short-range indoor communication systems in the frequency range 300 ~400 GHz have been carried out[12]. In this paper, a slow-wave structure of grating in a rectangular waveguide is proposed as the circuit for a BWO at 340 GHz with a sheet beam, due to its simple geometry that allows the easy realization. In Section II, the dispersion relation and the interaction impedance of the SWS are analyzed and computed, as well as compared with the results by

Received date: 2017-05-02, **revised date**: 2017-09-15 **收稿日期**:2017-05-02, **修回日期**:2017-09-15

Foundation items:Supported by the National Key Basic Research Program of China (2013CB933603), and China Scholarship Council

Biography:ZHANG Kai-Chun (1972-), male, Chengdu, doctor. Research area involves terahertz and millimeter wave devices

* **Corresponding author**:E-mail: zh.kch@163.com

CST simulation. In Section III, a PIC code CHIPIC[13] is adopted to simulate a sheet beam tunable BWO with this SWS at 340 GHz with very low current density.

1 Theoretical analysis

1.1 Dispersion relation

The schematic of the longitudinal section is shown in Fig. 1 with the width a in transverse and other geometric parameters denoted. Based on the analytical model in Ref. 14, the dispersion equation of the TE_{xlm} mode can be calculated via solving the wave equations in both the region I and region II by applying the continuity of tangential components of E-field and H-field on the interface between the two regions. Thus the dispersion equation of the dominant TE_{xlm} mode is written as:

$$1 - \frac{s}{d}\tan(v_x h)\sum_{n=-\infty}^{\infty}\frac{v_x}{v_n}\frac{\mathrm{sinc}^2(k_{zn}s/2)}{\tanh[v_n(b-h)]}, \quad (1)$$

where

$$\begin{cases} k_x = l\pi/a \quad l = 1,\cdots,\infty \\ v_x = \sqrt{k_0^2 - k_x^2} \\ k_{zn} = k_z + 2n\pi/d \quad n = 0, \pm 1, \cdots \pm \infty \\ v_n = \sqrt{k_{zn}^2 - v_x^2} \end{cases}$$

with the longitudinal wavenumber k_{zn} of the nth Floquet spatial harmonic and transverse wavenumbers k_x, ν_x and ν_n.

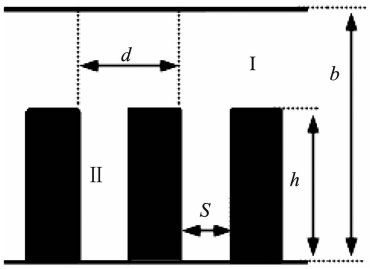

Fig. 1 Longitudinal section view of the SWS
图 1 慢波结构的纵向截面图

In the dispersion equation there exists a $\tan(v_x h)$ function related to the grating height h. A numerical calculation was performed to solve the dispersion relation Eq. 1. The geometric parameters corresponding to the frequency range 100 ~ 600 GHz assumed in the calculation are listed in Table 1.

Table 1 The geometric parameters (Unit in mm)
表 1 几何结构参数(单位:mm)

s	d	a	b	h
0.08	0.14	0.96	0.48	0.18

The fundamental TE_{x10} mode, the upper modes TE_{x20} and TE_{x30} varying with the wave number normalized to the period d of the grating are shown as Fig. 2. The calculation results by the analytical model are plotted in solid line. By comparison, the dispersion of these three modes, simulated by a full electromagnetic 3-D software CST, are plotted in dash line. The analysis results agree well with those by the simulation. The comparison infers the validation of the analytical method. The TE_{x10}, TE_{x20} and TE_{x30} mode exists in the range 150 ~ 370 GHz, 300 GHz- 460 GHz and 405 ~ 570 GHz, respectively.

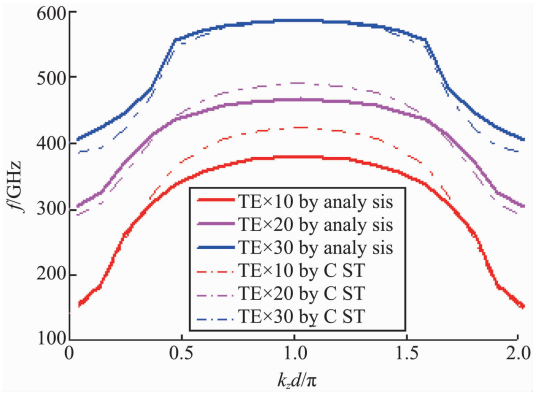

Fig. 2 Dispersion curves of the SWS by analysis and CST
图 2 理论分析和 CST 仿真的慢波结构色散曲线

Here we mainly discuss the dispersion of the fundamental mode TE_{x10} varying with grating width and height of the SWS. The dispersion curves of the mode with the geometric parameters are shown in Fig. 3. In these calculations, only the waveguide grating width and height are changed while others kept constant. The results in Fig. 3 (a), which display the dispersion curves related to the waveguide width (namely the grating width) a in the range of 0.90 ~ 1.00 mm, indicate that an increase of the grating width lowers the dispersion curves. Results in Fig. 3 (b) indicate that an increase of grating depth h in the range of 0.16 ~ 0.20 mm lowers the dispersion curve. Meanwhile the deeper grating can flatten the dispersion curve. By comparison the grating depth can strongly influence the dispersion, while the width lightly.

1.2 Interaction impedance

BWO working principle is based on the synchronisms of the electron velocity with the phase velocity of the first backward wave space harmonic of a slow-wave structure. The interaction impedance of the -1^{st} space harmonic is defined as:

$$K_{(-1)} = \frac{|E_{z(-1)}|^2}{2\beta_{(-1)}^2 P}, \quad (2)$$

where $E_{z(-1)}$ is the z-component of the electric field interacting with the electron beam, $\beta_{z(-1)}$ the propagation constant of the -1^{st} space harmonic, and P is the power of the propagating field including all the space harmonics.

The electromagnetic field expressions of the TE_{xmn} mode for the SWS is expressed as

$$\begin{bmatrix} E_x \\ E_y \\ E_z \end{bmatrix} = \frac{\omega\mu_0}{v_x^2}\sin(k_x x)\sum_{n=-\infty}^{\infty} a_n e^{ik_{zn}z} \begin{bmatrix} 0 \\ -k_{zn}\cosh[v_n(b-y)] \\ iv_n\sinh[v_n(b-y)] \end{bmatrix}$$

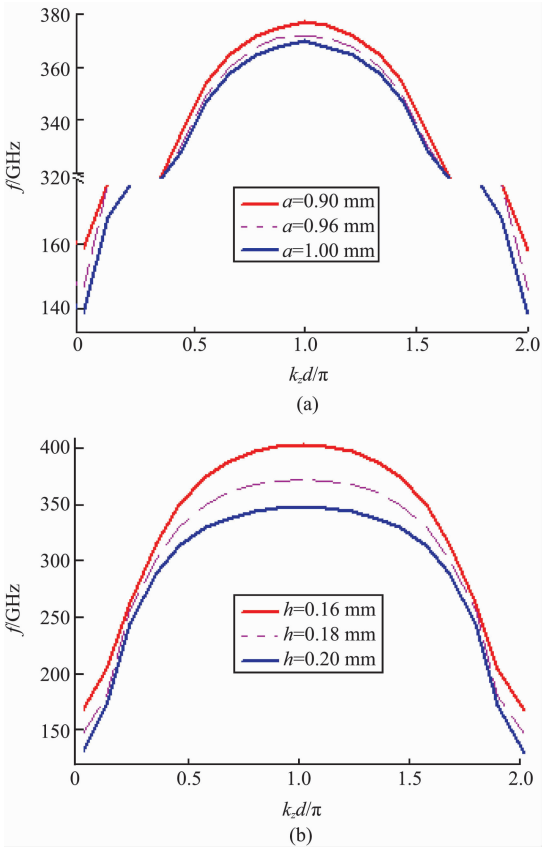

Fig. 3　Dispersion curves of the TE_{x10} mode with grating width (a) and height (b)

图 3　TE_{x10}模的色散曲线,随光栅宽度(a)和深度(b)的变化

$$\begin{bmatrix} H_x \\ H_y \\ H_z \end{bmatrix} = \sum_{n=-\infty}^{\infty} a_n \mathrm{e}^{ik_{zn}z} \begin{bmatrix} \sin(k_x x)\cosh[v_n(b-y)] \\ -\frac{k_x v_n}{v_x^2}\cos(k_x x)\sinh[v_n(b-y)] \\ i\frac{k_{zn} v_n}{v_x^2}\cos(k_x x)\cosh[v_n(b-y)] \end{bmatrix}, \quad (3)$$

where

$$a_n = \frac{b_0 s v_x \sin(v_x h)\,\mathrm{sinc}(k_n s/2)\,\mathrm{e}^{ik_{zn}s/2}}{v_n d\,\sinh[v_n(b-y)]}$$

Based on the field expression in Eq. 3, the interaction impedance for the -1^{st} space harmonic can be derived by calculating the Poynting flux and z-component of the electric field. After some algebraic manipulations, the square of the magnitude of z-component of the electric field is written:

$$|E_{z(-1)}|^2 = |b_0|^2\left(\frac{\omega\mu_0}{v_x}\right)^2\left(\frac{s}{d}\right)^2 \sin^2(v_x h)\sin^2(k_x x)\frac{\sinh^2[v_{(-1)}(b-y)]}{\sinh^2[v_{(-1)}(b-h)]}\mathrm{sinc}^2(k_{(-1)}s/2), \quad (4)$$

and the Poynting flux is expressed as:

$$P = -\frac{1}{8}|b_0|^2\omega\mu_0 a(b-h)\left(\frac{s}{d}\right)^2 \sin^2(v_x h)\sum_{n=-\infty}^{\infty}\frac{k_n}{v_n^2}\frac{\mathrm{sinc}^2(k_n s/2)}{\sinh^2[v_n(b-h)]}\left\{1+\frac{\sinh[2v_n(b-h)]}{2v_n(b-h)}\right\}. \quad (5)$$

Thus, the interaction impedance of the -1^{st} space harmonic is written as,

$$K_{(-1)} = K_{(-1)c}\sin^2(k_x x)\sinh^2[v_{(-1)}(b-y)], \quad (6)$$

where,

$$K_{(-1)c} = \frac{-4\omega\mu_0}{a(b-h)\beta_{(-1)}^2 v_x^2}\frac{\mathrm{sinc}^2(k_{(-1)}s/2)}{\sinh^2[v_{(-1)}(b-h)]}\frac{1}{\sum_{n=-\infty}^{\infty}\frac{k_n}{v_n^2}\frac{\mathrm{sinc}^2(k_n s/2)}{\sinh^2[v_n(b-h)]}\left\{1+\frac{\sinh[2v_n(b-h)]}{2v_n(b-h)}\right\}}$$

is a coefficient that depends on the geometric parameters, wavenumbers and operating frequency. The coefficient $K_{(-1)c}$ should have a minus. The maximum value of $K_{(-1)}$ is obtained assuming $x = a/2$ and $y = h$.

Here we specially focus on the impedance in the space $y \geqslant h$, where the electron sheet beam can effectively interact with the E-field above the grating. The interaction impedance, varying with the distance from the grating top for the first backward space harmonic by analysis in formula 6 and CST simulation, is shown in Fig. 4. The interaction impedance is computed in the range of 1.45 ~ 1.55 π on the line ($x = a/2$, $y = h$) and ($x = a/2$, $y = h + 0.05$ mm), respectively. These graphics indicate that the interaction impedance decreases with $k_z d$ in the range 1.45 ~ 1.55 π and sharply decreases with the distance from the grating top. The results show that the structure has high interaction impedance and that the results by analysis agree with those by simulation. Furthermore the impedance decreases about 20 times when the distance between the beam and the grating top increases from $y = h$ to $y = h + 0.05$ mm. In order to enhance the beam-wave interaction, the distance should be very small. On the other hand the results can provide the choice of the distance, which compromises between avoiding beam being caught by the grating and achieving the highest interaction impedance.

2　PIC simulation

By optimizing the dispersion and impedance, the dimension of the SWS for a 340GHz BWO are determined in Table 1. A BWO, to be tunable, requires the beam line to intercept the -1^{st} backward wave of the dispersion curve. When the electron energy lies in 10 ~ 18 keV, the beam line can intercept the dispersion curve of the TE_{x10} mode in a frequency range of 330 ~ 366 GHz in Fig. 2.

The BWO performance is simulated using a 3-D PIC code CHIPIC. The SWS consists of 60 periods (8.4mm length). The structure is considered to be made of free-oxide copper (conductivity 5.8×10^7 S/m). The BWO is initially simulated at the central frequency 340 GHz and a beam voltage 12.8 kV. A sheet electron beam

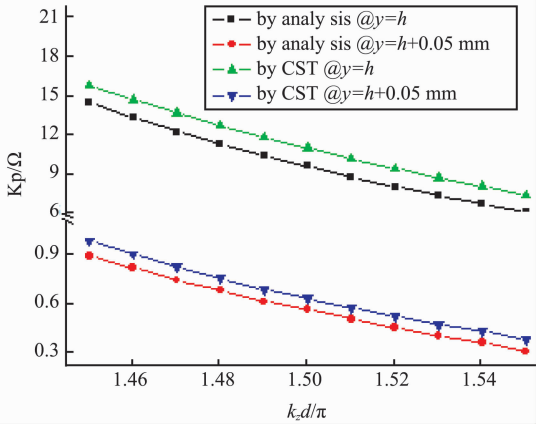

Fig. 4 Interaction impedance varying with h
图 4 互作用阻抗随 h 的变化

800 μm × 80 μm, whose central position in y-direction is 50 μm above the grating top, is adopted and the distance between the beam and the grating is 10 μm. The beam current 6.4 mA (current density 10 A/cm^2) is chosen to compromise the maximum output power and the recent cathode emitting ability without e-beam convergence. Due to the short transmission length of the beam and low current density, the magnet required is not too strong. A uniform solenoid focusing magnetic field of 0.3 T can meet the requirement for beam confinement and noncollision with the grating. The power spectrum of the BWO output signal is shown in Fig. 5, which has an output peak power more than 100 mW at the frequency 340 GHz.

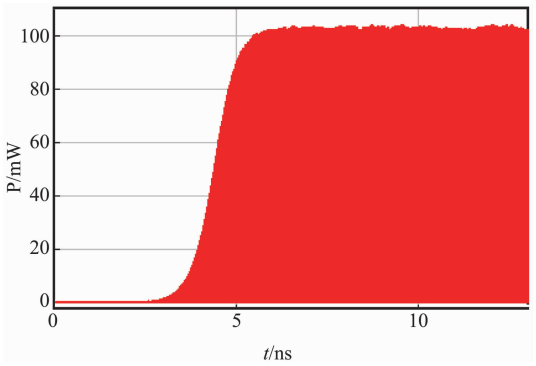

Fig. 5 Output power spectrum
图 5 输出功率谱

To demonstrate the tunable performance of the BWO, different cathode voltages 10 ~ 18 kV are considered while the beam current, period numbers and the focusing magnetic field are maintained fixed at the original values. The frequency and power of the BWO increase with the voltage as shown in Fig. 6. From Fig. 4 the interaction impedance decreases with the phase shift in the range 1.45 ~ 1.55π. Then from Fig. 3 the interaction impedance actually increases with the voltage and the frequency in this range. The increase both in the interaction impedance and bean energy enhances the beam-wave interaction in the voltage range. The BWO delivers the output power 30 ~ 350 mW from 325 GHz to 355 GHz with

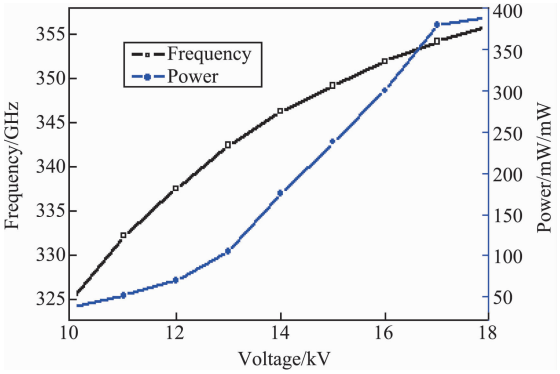

Fig. 6 Frequency excited and output power with voltage
图 6 激发频率和输出功率随电压的变化

30 GHz tunable bandwidth.

For THz BWO, the product of ISTOK presents the best level. Its output power is less than 10 mW near 340 GHz with the voltage less than 6 kV[15]. On other hand, Mineo M[16] adopted this type SWS to study 0.9 ~ 1.1 THz BWO and predicted to deliver more than 100 mW with the current density 500 A/cm^2 (current 8 mA). By comparison, our BWO model has great advantages in the high output power and the low current density.

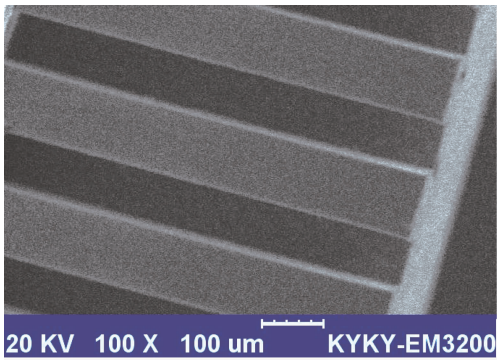

Fig. 7 Fabrication sample by LIGA
图 7 经 LIGA 加工的高频结构样品

Fabrication of the SWS is a major challenge because the physical dimensions of the SWS are inherently small. This imposes severe constraints on the fabrication tolerance and surface roughness of several skin depths in order to minimize the losses in the electromagnetic wave propagation path. A microfabrication of Lithographie Galvanoformung Abformung (LIGA) technology in Being Synchrotron Radiation Facility (BSRF) was adopted to manufacture the slow-wave structure. The fabricated sample is shown in Fig. 7 with good fabrication uniformity and surface roughness, which verifies the fabrication of the SWS used in the THz range.

3 Conclusions

A slow-wave structure comprising a rectangular waveguide with a grating has been analyzed. The slow-wave dispersion relation and the interaction impedance were derived and numerically solved. The validity of the

analytical model is verified by comparison with 3-D electromagnetic software. Because The SWS has attractive merit in high interaction impedance and micro-fabrication, it is adopted as the circuit for BWO in THz band. A tunable BWO, operating in the range of 325 ~ 355 GHz range, is demonstrated as a promising vacuum source for terahertz signal generation. The BWO is predicted to deliver more than several tens or several hundreds of mW with a lower current density. It has a promising application for wireless communication at 340 GHz.

References

[1] Chattopadhyay G. Technology, capabilities, and performance of low power terahertz sources [J]. *IEEE Trans. Terahertz Sci. Technol.* 2011, **1**(1): 33 - 53.

[2] Liu Y Q, Kong L B, Du C H, *et al*. A terahertz electronic source based on the spoof surface plasmon with Subwavelength Metallic Grating [J]. *IEEE Trans. Plasma Sci.*, 2016, **44**(6): 930 - 937.

[3] Cai J, Wu X, Feng J. Traveling-wave tube harmonic amplifier in terahertz and experimental demonstration [J]. *IEEE Trans. Electron Devices*, 2015, **62**(2): 648 - 651.

[4] Zhang K C, Wu Z H, Liu S G. Study of a rectangular coupled cavity extended interaction oscillator in sub-terahertz waves [J]. *Chinese Physics B*, 2008, **17**(9): 3402 - 3406.

[5] Herman M A, Strohmer T. High-resolution radar via compressed sensing [J]. *IEEE Transactions on Signal Processing*, 2009, **57**(6): 2275 - 2284.

[6] Liu W, Zhao C, Li K, *et al*. Two-section folded-waveguide slow-wave structure for terahertz extended interaction oscillator [J]. *IEEE Trans. Electron Devices*. 2014, **61**(3): 902 - 908.

[7] Tucek J, Gallagher D, Kreischer K, *et al*. A compact, high power, 0.65 THz source [C]. 2008 *IEEE Int. Vac. Electron. Conf.*, 2008, **60008**: 16 - 17.

[8] Paoloni C, Carlo A D, Brunetti F, *et al*. Design and fabrication of a 1 THz backward wave amplifier [J]. *Terahertz Sci. Technol.*, 2011, **4**(4): 149 - 163.

[9] Wang C, Lu B, Lin C, *et al*. 0.34 THz wireless link based on high-order modulation for future wireless local area network applications [J]. *IEEE Trans. Terahertz Sci. Technol.*, 2014, **4**(1): 75 - 85.

[10] Song H J, Nagatsuma T. Present and future of terahertz communications [J]. *IEEE Trans. Terahertz Science & Technol.*, 2011, **1**(1): 256 - 263.

[11] Koenig S, Lopezdiaz D, Antes J, *et al*. Wireless sub-THz communication system with high data rate[J]. *Nature Photonics*, 2013, **7**(12): 977 - 981.

[12] Zhang K C, Qi Z K, Yang Z L. A novel multi-pin rectangular waveguide slow-wave structure based backward wave amplifier at 340 GHz [J], *Chinese Phys. B*. 2015, **24**(7): 79402.

[13] Zhou J, Liu D, Liao C, *et al*. CHIPIC: An efficient code for electromagnetic PIC modeling and simulation [J]. *IEEE Trans. Plasma Sci.*, 2009, **37**(10): 2002 - 2011.

[14] Basten M A, Booske J H, Joe J, *et al*. Analysis of rectangular waveguide-gratings for amplifier applications [J]. *IEEE Trans. Microw. Theory Tech.*, 1994, **42**(6): 995 - 1003.

[15] http://www.istok.com.cn

[16] Mineo M, Paoloni C. Corrugated rectangular waveguide tunable backward wave oscillator for terahertz applications[J]. *IEEE Trans. Electron Devices*, 2010, **57**(6): 1481 - 1484.